SUPPORTING INFORMATION

Investigating the Structural Dynamics of the α-1,4-Galactosyltransferase LgtC from *Neisseria meningitidis* by NMR Spectroscopy †

Patrick H. W. Chan[‡§], Adrienne H. Cheung[‡], Mark Okon[‡||], Hong-Ming Chen[||], Stephen G. Withers[‡§||], Lawrence P. McIntosh[‡§||⊥*]

[‡]Department of Biochemistry and Molecular Biology, University of British Columbia, Vancouver BC, V6T 1Z3

[§]Centre for High-throughput Biology, University of British Columbia, Vancouver BC, V6T 1Z4

[||]Department of Chemistry, University of British Columbia, Vancouver BC, V6T 1Z1

[⊥]Michael Smith Laboratories, University of British Columbia, Vancouver BC, V6T 1Z4

TABLES

Table S1: Steady state kinetic parameters for UAA-labeled LgtC.

	[c] UDP-Gal			[d] Lactose		
	K_m (μM)	k_{cat} (s^{-1})	k_{cat}/K_m ($\mu M^{-1}\ s^{-1}$)	K_m (mM)	k_{cat} (s^{-1})	k_{cat}/K_m ($mM^{-1}\ s^{-1}$)
CF_3Phe-labeled LgtC-F132X [a]	14	33	2.4	29	35	1.2
$O^{13}CH_3$Phe-labeled LgtC-F132X [a]	10	29	3.1	14	40	2.8
WT LgtC [a]	19	46	2.5	-	-	-
WT LgtC [b]	29	16	0.6	101	23	0.2

[a] Kinetic assays carried out with protein in 20 mM HEPES, 50 mM KCl, 15 mM $MnCl_2$, 0.5 mM NADH, 0.1% bovin serum albumin (BSA), 0.7 mM phosphoenolpyruvate (PEP), 5 mM DTT, 2.7 units lactate dehydrogenase (LDH), 2.2 units pyruvate kinase (PK) at pH 7.5 and 30 °C, as described previously.[1]

[b] As above except at 25 °C (reproduced from Table 1 of Chan et al., 2012[1])

[c] Data for sugar donor UDP-Gal in the presence of 160 mM acceptor lactose.

[d] Data for sugar acceptor lactose in the presence of 10 mM donor UDP-Gal.

FIGURES

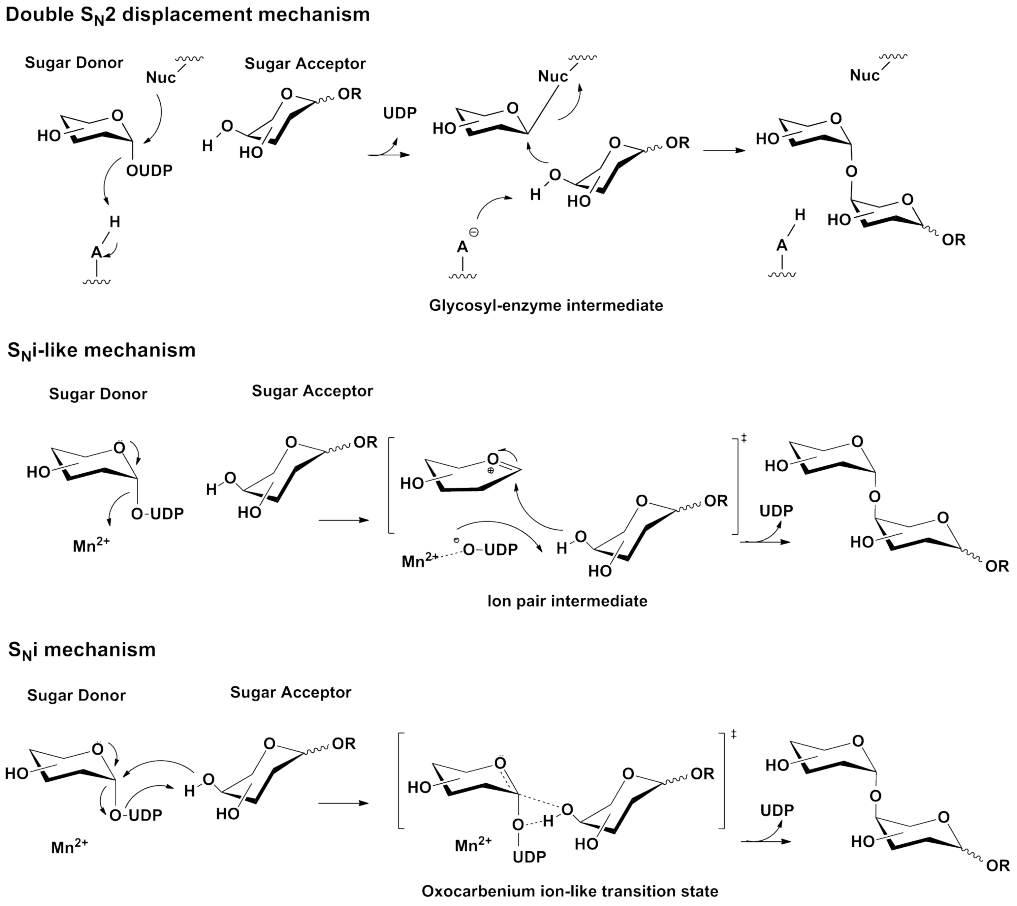

Figure S1: Suggested reaction mechanisms followed by the retaining glycosyltransferase LgtC: (A) double displacement S_N2 (bimolecular nucleophilic substitution) with two sequential Walden inversions and covalent glycosyl-enzyme intermediate, (B) S_Ni-like, and (C) S_Ni. The latter "internal return" nucleophilic substitutions involve a front-side attack to yield net retention of stereochemistry at the donor anomeric carbon. Based on extensive kinetic analyses and molecular stimulations,[2-6] LgtC appears to follow the S_Ni-like mechanism involving a short-lived oxocarbenium ion-like intermediate with stabilization by the UDP leaving group phosphate. (A: general acid; Nuc: nucleophile; adapted from Lairson et al.[7])

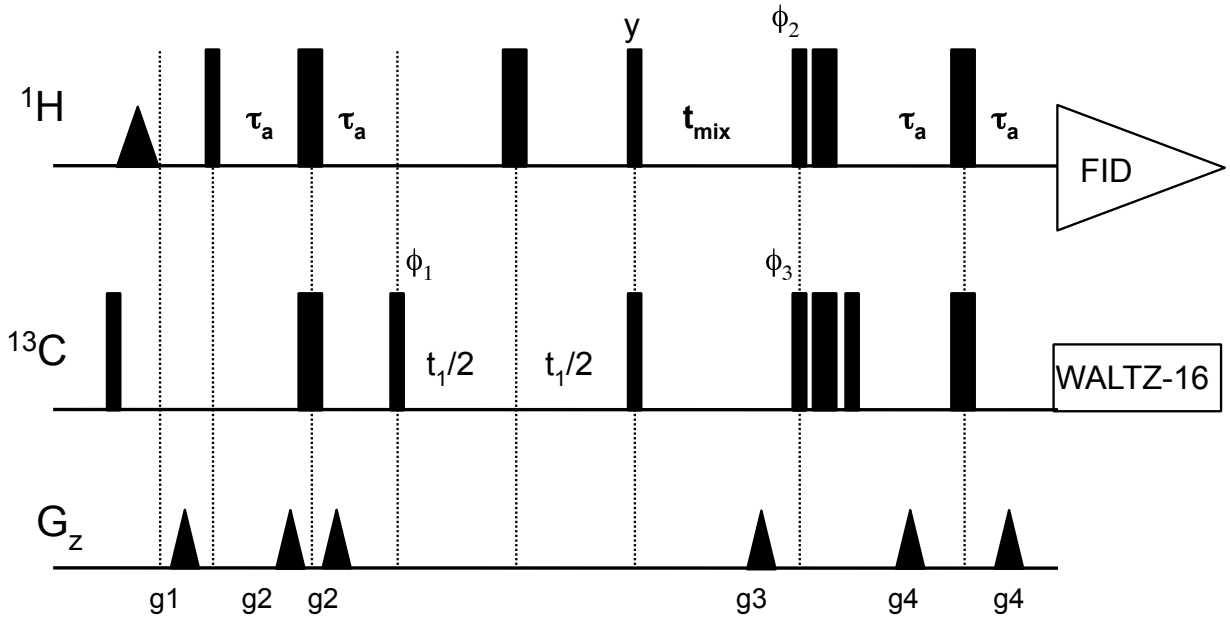

Figure S2: Methyl-TROSY-based pulse sequence for the measurement of conformation exchange via transfer of H_zC_z magnetization. Narrow (or wide) pulses have flip angles of 90^o (or 180^o) degrees and τ_a = 1.8 msec. The first proton pulse is 6.8 msec Eburp1 90^o applied at the frequency of water. Afterwards, the ^{1}H transmitter frequency is shifted to the middle of methyl region (0.9 ppm). The ^{13}C transmitter frequency is at the middle of the methyl region (19 ppm). The phase cycles are ϕ_1 = x, -x; ϕ_2 = 2(x), 2(-x); ϕ_3 = 4(x), 4(-x); and Receiver = x, 2(-x), x, -x, 2(x), -x. The durations and strengths of the gradients (with trapezoidal shapes) are g1 = 1 ms, 14 G/cm; g2 = 500 μs, 18.8 G/cm; g3 = 1 ms, 28.1 G/cm; g4 = 600 μs, 22.5 G/cm. This pulse sequence was provided by Dr. Lewis Kay (Univ. Toronto) and is described in Sprangers et al. [8]

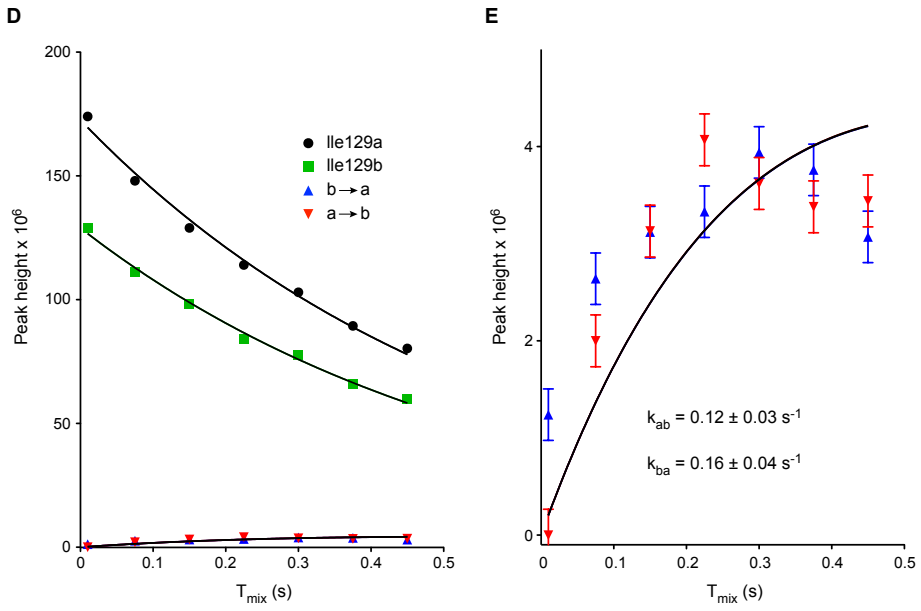

Figure S3: Analysis of the slow exchange between the "a" and "b" forms of Ile129. The above figure is reproduced from Figures 5D and 5E of the main text. The original spectra were processed in NMRPipe with Lorentzian-to-Gaussian apodization, and the nlinLS routine (http://spin.niddk.nih.gov/NMRPipe/ref/prog/nlinls.html) used to extract heights (or equivalently, volumes) and rms errors of Gaussian peaks, best fit for each signal over the entire time series.[9] The resulting heights of the auto peaks ($I_a(t)$ and $I_b(t)$ for the "a" and "b" methyl signals, respectively) and exchange peaks ($I_{ab}(t)$ and $I_{ba}(t)$ for the "a→b" and "b→a" signals, respectively) were analyzed according to the following equations from Farrow et al.:[10]

$$I_a(t) = I_a(0)\left\{-(\lambda_- - r_a)\, e^{-\lambda_+ t} + (\lambda_+ - r_a)\, e^{-\lambda_- t}\right\} / \{\lambda_+ - \lambda_-\}$$

$$I_b(t) = I_b(0)\left\{-(\lambda_- - r_b)\, e^{-\lambda_+ t} + (\lambda_+ - r_b)\, e^{-\lambda_- t}\right\} / \{\lambda_+ - \lambda_-\}$$

$$I_{ab}(t) = I_a(0)\left\{-k_{ab}\, e^{-\lambda_+ t} + k_{ab}\, e^{-\lambda_- t}\right\} / \{\lambda_+ - \lambda_-\}$$

$$I_{ba}(t) = I_b(0)\left\{-k_{ba}\, e^{-\lambda_+ t} + k_{ba}\, e^{-\lambda_- t}\right\} / \{\lambda_+ - \lambda_-\}$$

where

$$\lambda_{+,-} = \{(r_a + r_b) \pm [(r_a - r_b)^2 + 4k_{ab}k_{ba}]^{1/2}\}/2$$

and $r_a = R_a + k_{ab}$ and $r_b = R_b + k_{ba}$. Here, R_a and R_b are the effective relaxation rate constants of the H_zC_z two-spin longitudinal coherences of the "a" and "b" states, and k_{ab} and k_{ba} are the rate constants for the conformational exchange. Ideally, $I_{ab}(t) = I_{ba}(t)$ and the equilibrium constant for two-site exchange $K_{eq} = I_a(0) / I_b(0) = k_{ba} / k_{ab}$. However, due to differential relaxation ($R_a \neq R_b$) over the time course of the pulse sequence and insufficiently long recovery delays, peak heights may not reflect equilibrium populations. Therefore, using Prism GraphPad, the auto and exchange peaks (weighted by the nlinLS rms height errors of ~2.65 x 10^5, shown as error bars in panel E and smaller than the symbols in D) were simultaneously non-linearly least squares fit to obtain 6 independent parameters, tabulated below.

Parameter	Best fit value	Standard error	95% confidence intervals
k_{ab}	0.12 s^{-1}	0.029 s^{-1}	0.060 to 0.18 s^{-1}
k_{ba}	0.16 s^{-1}	0.039 s^{-1}	0.081 to 0.24 s^{-1}
$I_a(0)$	1.73 x 10^8	1.54 x 10^6	1.70 x 10^8 to 1.76 x 10^8
$I_b(0)$	1.29 x 10^8	1.54 x 10^6	1.26 x 10^8 to 1.32 x 10^8
R_a	1.65 s^{-1}	0.052 s^{-1}	1.54 to 1.76 s^{-1}
R_b	1.61 s^{-1}	0.069 s^{-1}	1.46 to 1.75 s^{-1}

Although not constrained, it is noteworthy $k_{ba} / k_{ab} = 1.33$ and $I_a(0) / I_b(0) = 1.34$ as $R_a \sim R_b$. The errors, which reflect fit precision, are determined from standard algorithms using the residuals and the covariance matrix (e.g., see http://graphpad.com/guides/prism/6/curve-fitting/).

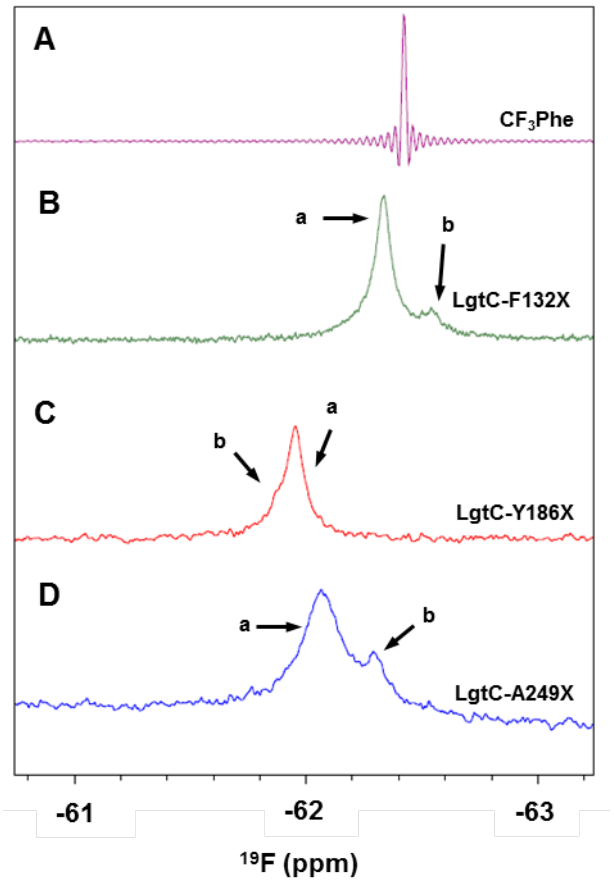

Figure S4: The ^{19}F-NMR spectra of (A) free CF_3Phe and CF_3Phe-labeled *apo* proteins: (B) LgtC-F132X, (C) LgtC-Y186X, and (D) LgtC-A249X. Two signals ("a" and "b") are observed for each protein sample, indicative of at least two conformational states detectable by the ^{19}F reporter nuclei at three side-chain positions in LgtC. The differences in the "a" versus "b" peak intensity ratios for the three LgtC samples suggests that the observed conformational heterogeneity is more complex than a simple two-state equilibrium.

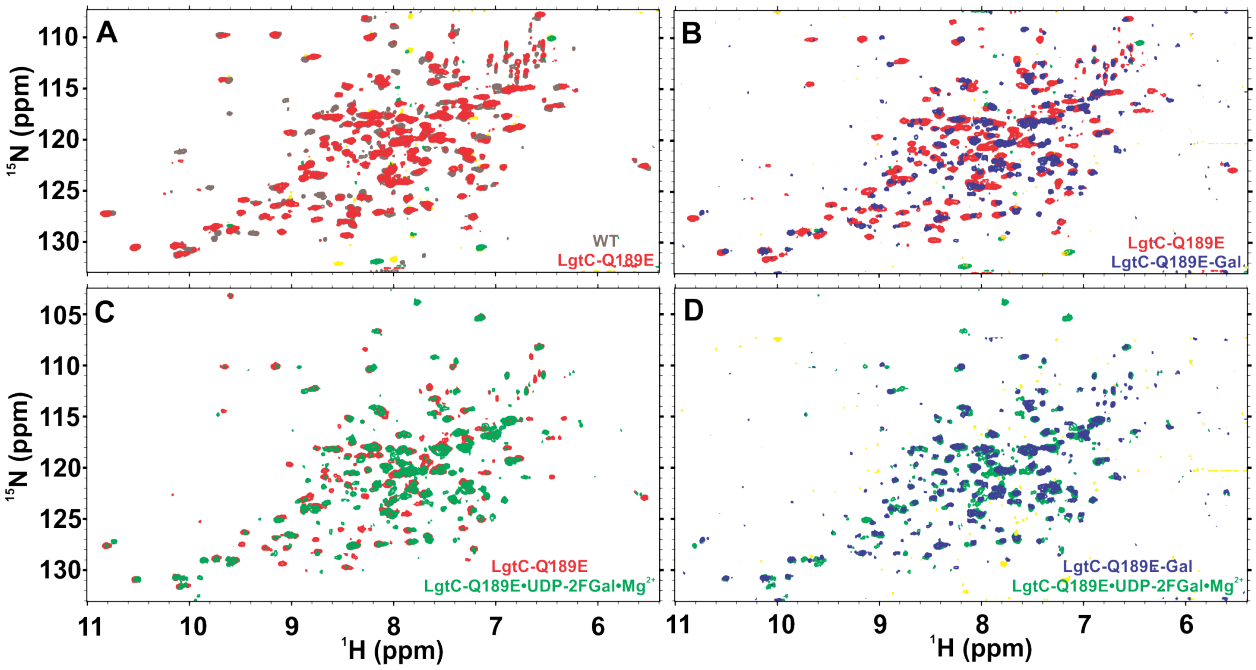

Figure S5: (A) Overlaid ^{15}N-TROSY-HSQC spectra of ^{15}N-labeled LgtC-Q189E (red, green) and wild-type LgtC (grey, yellow). The aliased peaks (yellow, green) result from the reduced ^{15}N spectral width. The spectra indicate that LgtC-Q189E adopts a wild-type-like structure, yet significant spectral perturbations also suggest conformational perturbations due to the Q189E point mutation. The ^{15}N-TROSY-HSQC spectrum of wild-type LgtC has only been partially assigned. (B-D) Overlaid spectra comparing *apo* LgtC-Q189E (red, aliased peaks in green), its binary complex with UDP-2FGal•Mg^{2+} (green), and its covalent glycosyl-enzyme intermediate LgtC-Q189E-Gal (blue, aliased in yellow) show chemical shift perturbations due to donor analog binding and covalent modification of Asp190, respectively. ESI-MS analysis of *apo* LgtC-Q189E indicates the presence of some glycosyl-enzyme intermediate. The spectrum of LgtC-Q189E-Gal was recorded 15 minutes after incubation with UDP-Gal•Mg^{2+} in the presence of pyruvate kinase and phosphoenolpyruvate to deplete UDP and thereby enrich the covalent intermediate.

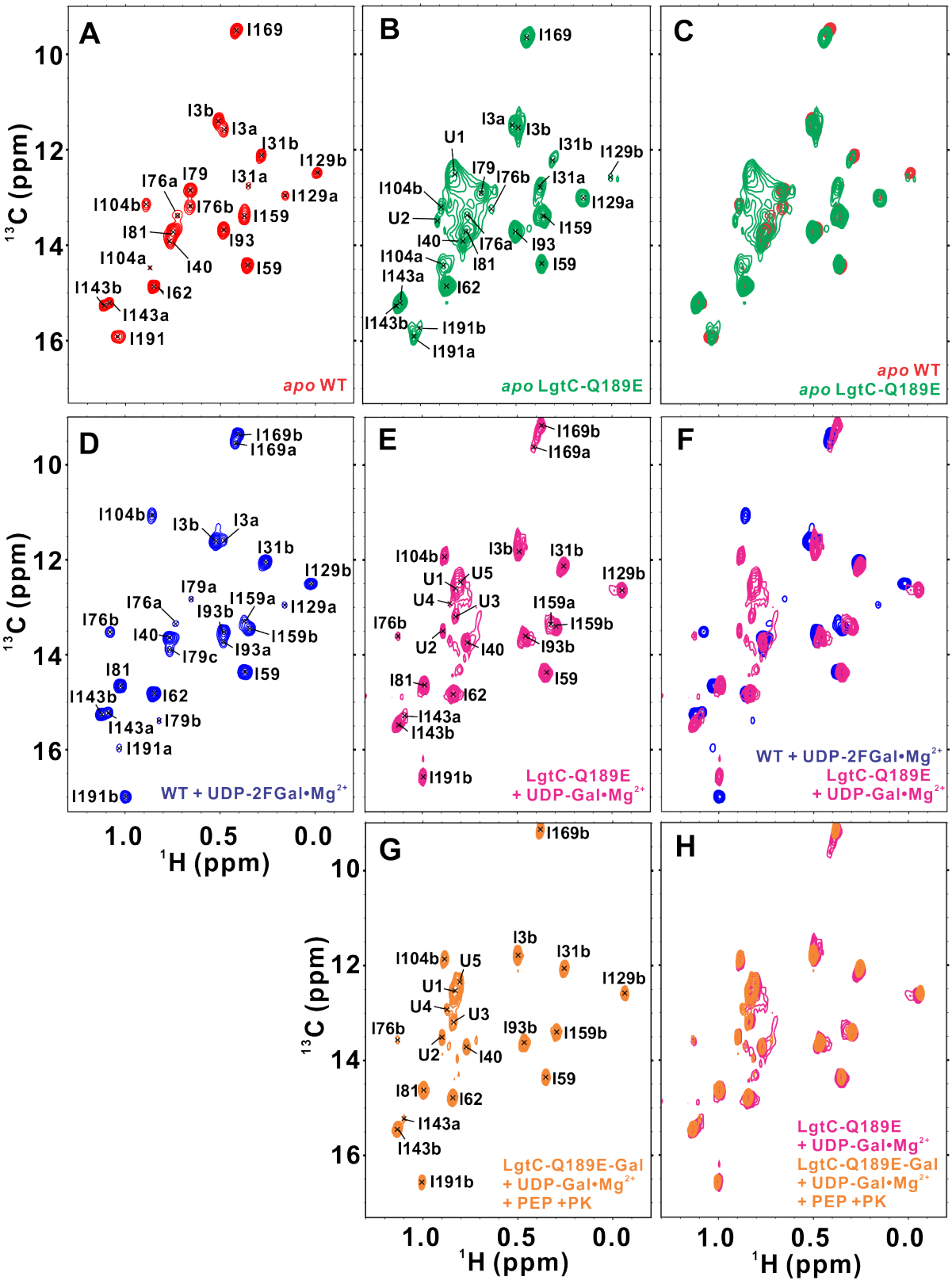
A
I169
I3b
I3a
I31b
I129b
I76a
I79
I31a
I129a
I104b
I76b
I159
I81
I93
I104a
I40
I59
I143b
I62
I143a
I191
apo WT
B
I169
I3a
I3b
U1
I31b
I129b
I79
I76b
I31a
I104b
I129a
U2
I159
I40
I76a
I93
I104a
I81
I59
I143a
I62
I143b
I191b
I191a
apo LgtC-Q189E
C
apo WT
apo LgtC-Q189E
D
I169b
I169a
I104b
I3b
I3a
I31b
I129b
I79a
I76a
I159a
I93b
I129a
I76b
I40
I159b
I79c
I93a
I81
I59
I143b
I62
I143a
I79b
I191a
I191b
WT + UDP-2FGal•Mg2+
E
I169b
I169a
I104b
I3b
I31b
I129b
U1
U5
U4
U3
I159a
I76b
I159b
U2
I40
I93b
I81
I59
I62
I143a
I143b
I191b
LgtC-Q189E
+ UDP-Gal•Mg2+
F
WT + UDP-2FGal•Mg2+
LgtC-Q189E
+ UDP-Gal•Mg2+
G
I169b
I3b
I104b
U5
I31b
U1
I129b
U4
U3
I76b
I93b
I159b
U2
I40
I59
I81
I62
I143a
I143b
I191b
LgtC-Q189E-Gal
+ UDP-Gal•Mg2+
+ PEP +PK
H
LgtC-Q189E
+ UDP-Gal•Mg2+
LgtC-Q189E-Gal
+ UDP-Gal•Mg2+
+ PEP +PK
10
12
14
16
13C (ppm)
1.0
0.5
0.0
1H (ppm)

Figure S6: Comparison of methyl-TROSY spectra of wild-type LgtC and the LgtC-Q189E mutant. Shown are spectra of the *apo* forms of (A) wild-type LgtC and (B) LgtC-Q189E separately and (C) overlaid. The spectra indicate that the two proteins are similar except for two unassigned peaks (U1 and U2) are observed in mutant. ESI-MS analysis of *apo* LgtC-Q189E indicates the presence of some glycosyl-enzyme intermediate. Also shown are spectra of the binary complexes of (D) wild-type LgtC with 1 mM UDP-2FGal and 10 mM Mg^{2+} and (E) LgtC-Q189E with 20 mM UDP-Gal and 10 mM Mg^{2+}. Since hydrolysis of the natural substrate might occur with LgtC-Q189E, the reaction was incubated for only 10 min. before spectra acquisition. When overlaid (F), chemical shift perturbations are seen which may reflect differences between the two sugar donors, structural differences between the proteins, and the possible presence of some covalently-modified LgtC-Q189E-Gal. A higher population of the LgtC-Q189E-Gal covalent glycosyl-enzyme intermediate was generated by addition of 50 mM phosphoenolpyruvate (PEP) and 15 units of pyruvate kinase (PK) to deplete any UDP, and its spectrum is shown in (G). Spectral comparison (H) reveals that the latter contains a single population of modified species, whereas the starting binary complex is heterogeneous. The spectra of LgtC-Q189E were assigned based on peak overlap with those of the wild-type protein.

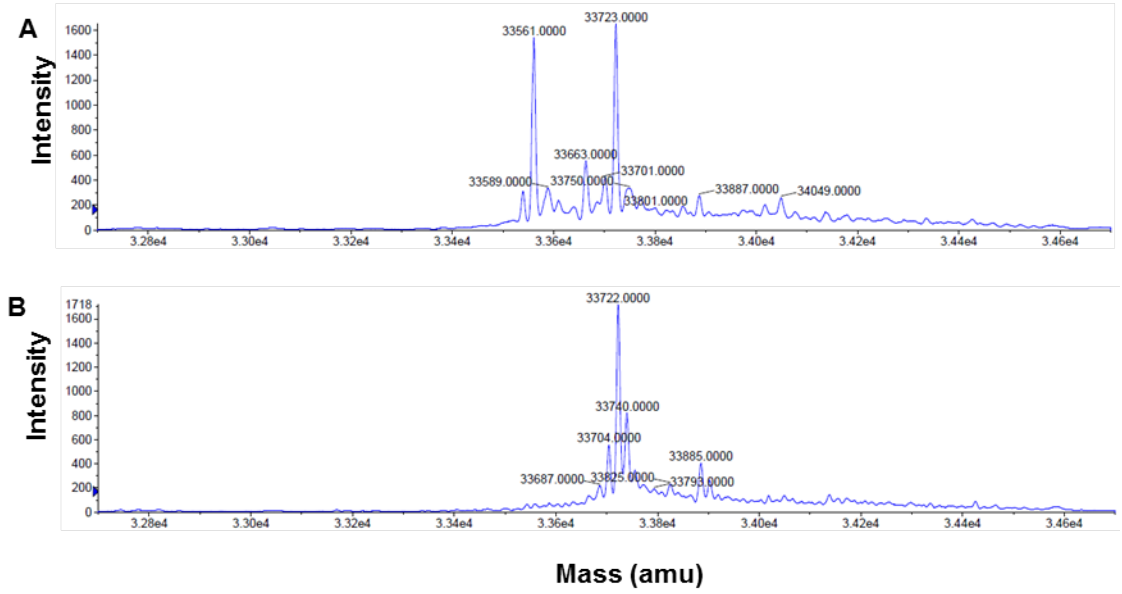

Figure S7: ESI-MS spectra of ^{15}N-labeled (A) LgtC-Q189E and (B) LgtC-Q189E-Gal. The 162 Da mass difference between peaks is consistent with a covalently-linked galactose. Note that the initial LgtC-Q189E appears partially modified possibly due to endogenous UDP-Gal in the *E. coli* expression cells. The LgtC-Q189E-Gal was formed by addition of 20 mM UDP-Gal, 10 mM $MgCl_2$, 50 mM phosphoenolpyruvate and 15 units of pyruvate kinase to deplete any UDP.

SUPPLEMENTAL REFERENCES

(1) Chan, P. H. W., Weissbach, S., Okon, M., Withers, S. G., and McIntosh, L. P. (2012) NMR spectral assignments of α-galactosyltransferase LgtC from *Neisseria meningitidis*: substrate binding and multiple conformational states. *Biochemistry 51*, 8278-8292.

(2) Persson, K., Ly, H. D., Dieckelmann, M., Wakarchuk, W. W., Withers, S. G., and Strynadka, N. C. (2001) Crystal structure of the retaining galactosyltransferase LgtC from *Neisseria meningitidis* in complex with donor and acceptor sugar analogs. *Nat. Struct. Biol*. *8*, 166-175.

(3) Ly, H. D., Lougheed, B., Wakarchuk, W. W., and Withers, S. G. (2002) Mechanistic studies of a retaining α-galactosyltransferase from *Neisseria meningitidis*. *Biochemistry 41*, 5075-5085.

(4) Tvaroska, I. (2004) Molecular modeling insights into the catalytic mechanism of the retaining galactosyltransferase LgtC. *Carbohydr Res. 339*, 1007-1014.

(5) Lee, S. S., Hong, S. Y., Errey, J. C., Izumi, A., Davies, G. J., and Davis, B. G. (2011) Mechanistic evidence for a front-side, S_Ni-type reaction in a retaining glycosyltransferase. *Nat. Chem. Biol. 7*, 631-638.

(6) Gomez, H., Polyak, I., Thiel, W., Lluch, J. M., and L., M. (2012) Retaining glycosyltransferase mechanism studied by QM/MM method: LgtC transfers alpha-galactose via an oxocarbenium ion-like transition state. *J. Am. Chem. Soc. 134*, 4743-4752.

(7) Lairson, L. L., Henrissat, B., Davies, G. J., and Withers, S. G. (2008) Glycosyltransferases: structures, functions, and mechanisms. *Ann. Rev. Biochem*. *77*, 521-555.

(8) Sprangers, R., Gribun, A., Hwang, P. M., Houry, W. A., and Kay, L. E. (2005) Quantitative NMR spectroscopy of supramolecular complexes: dynamic side pores in ClpP are important for product release. *Proc. Natl. Acad. Sci. USA 102*, 16678-16683.

(9) Delaglio, F., Grzesiek, S., Vuister, G. W., Zhu, G., Pfeifer, J., and Bax, A. (1995) NMRPipe: a multidimensional spectral processing system based on UNIX pipes. *J. Biomol. NMR 6*, 277-293.

(10) Farrow, N. A., Zhang, O., Forman-Kay, J. D., and Kay, L. E. (1994) A heteronuclear correlation experiment for simultaneous determination of ^{15}N longitudinal decay and chemical exchange rates of systems in slow equilibrium. *J. Biomol. NMR 4*, 727-734.